Neuron, Volume *94*

Supplemental Information

Homeostatic Plasticity Shapes Cell-Type-Specific Wiring in the Retina

Nai-Wen Tien, Florentina Soto, and Daniel Kerschensteiner

SUPPLEMENTARY INFORMATION

Homeostatic plasticity shapes cell-type-specific wiring in the retina

Nai-Wen Tien, Florentina Soto, Daniel Kerschensteiner

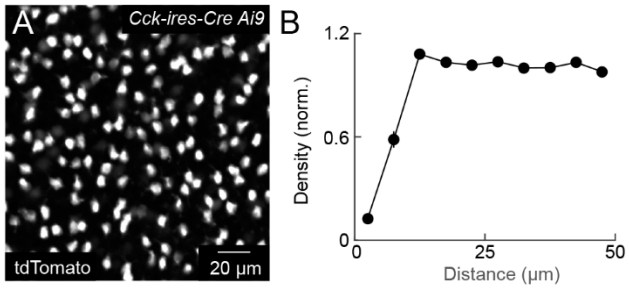

Figure S1. Distribution of tdTomato-expressing bipolar cells in *Cck-ires-Cre Ai9* (related to Figure 1)

(A) Representative confocal image of tdTomato-expressing cells in the bipolar cell body layer of a P21 whole-mount *Cck-ires-Cre Ai9* retina. (B) Summary data of the density recovery profiles of tdTomato-expressing cells in the bipolar cell body layer (n = 5 retinas) show an exclusion zone characteristic of labeling of a single cell type.

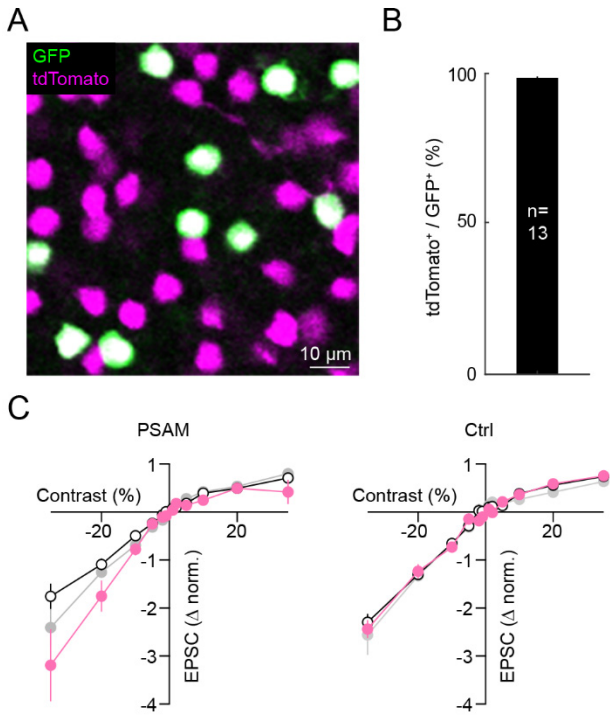

Figure S2. Pharmacogenetic silencing of B6 cells changes contrast response functions of ONα-RGCs (related to Figure 1)

(A) Representative image of the INL in a *CCK-ires-Cre Ai9* mouse injected with *AAV-Grm6$_s$-GFP*. (B) 98.5% ± 0.5 of GFP-positive cells in the INL were also tdTomato positive. (C) Contrast response functions of the normalized excitation of ONα-RGCs with (*PSAM*, n = 10) or without (*Ctrl*, n = 9) *AAV-Grm6$_s$-PSAM^{con}* injection before (*Before, black*), during (*PSEM, pink*) and after (*Wash, grey*) the addition of PSEM^{308}. Differences between responses before and during PSEM^{308} application in the *AAV-Grm6$_s$-PSAM^{con}* injected retinas were significantly different (95% confidence interval, see STAR Methods).

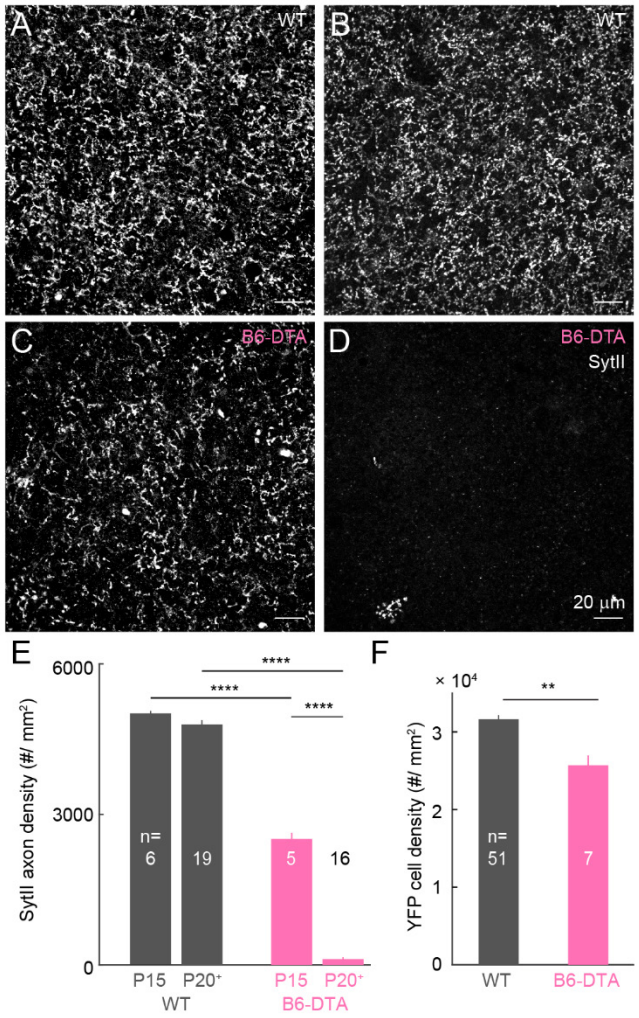

Figure S3. Cell-type-specific removal of B6 cells in *B6-DTA* mice (related to Figure 2)

(A-D) Representative images of SytII staining in the ON sublamina of the inner plexiform layer in P15 (A), P20^{+} (i.e. P20 – P30) (B) wild-type and P15 (C) and P20^{+} (D) *B6-DTA* retinas. (E) Summary data of the density of SytII-positive axons in the ON sublamina in wild-type and *B6-DTA* retinas during development. In (E), *P15 WT*: 5015 ± 50 # / mm^2; *P20^{+} WT*: 4792 ± 89 # / mm^2; *P15 B6-DTA*: 2511 ± 124 # / mm^2; *P20^{+} B6-DTA*: 115 ± 40 # / mm^2; *P15 WT* vs *P20^{+} WT* p = 0.48; *P15 WT* vs *P15 B6-DTA* p = 5 * 10^{-6}; *P20^{+} WT* vs *P20^{+} B6-DTA* p = 8 *10^{-26}; *P15 B6-DTA* vs *P20^{+} B6-DTA* p = 10^{-5}. (D) Summary data of the density YFP-expressing cells in wild-type (31624 ± 548 # / mm^2) and *B6-DTA* (25699 ± 1269 # / mm^2, p = 0.002) retinas.

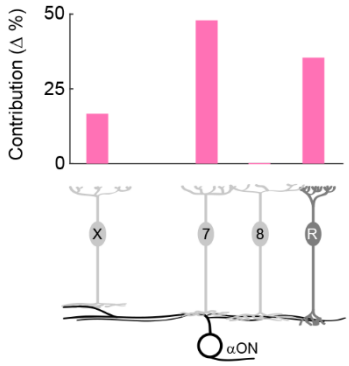

Figure S4. Bipolar cell types rewire with ONα-RGC in cell-type-specific ratios in *B6-DTA* mice (related to Figures 3, 4 and 5)

In *B6-DTA* mice, the number of excitatory synapses numbers on ONα-RGCs is reduced by 29.5 % compared to wild-type littermates. Given that B6 cells were shown to account for 70 % of the excitatory synapses on ONα-RGCs in wild-type retinas (Schwartz et al., 2012), it follows that non-B6 bipolar cells restore 40.5 % of the lost synapses in *B6-DTA* retinas. We calculated the approximate convergence of each bipolar cell type to ONα-RGCs by dividing the dendritic territory of the later by the axonal territory of the former. We then multiplied the convergence factor by the change in synapses numbers between pairs of individual bipolar cells and ONα-RGCs, to estimate the relative contribution each bipolar cell type to rewiring (XBC 17%, B7 47.4 %, RBC 35.6 %).

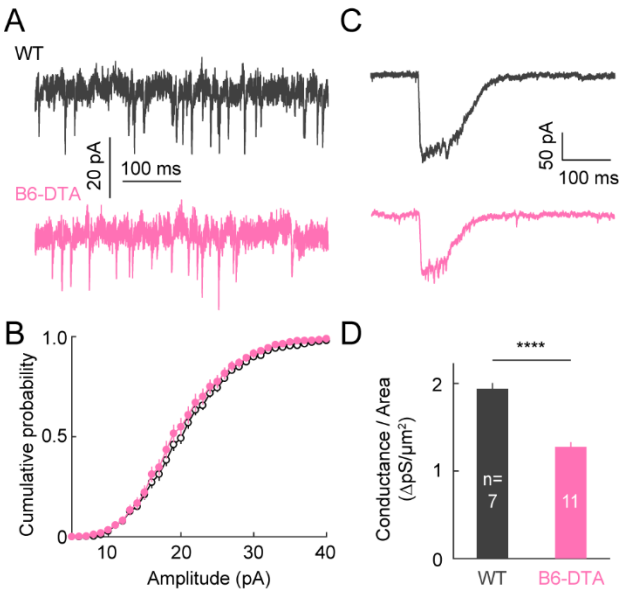

Figure S5. Postsynaptic strength in ONα-RGCs of *B6-DTA* mice (related to Figures 6 and 7) (A and B) Representative traces (A) and cumulative distribution curves (B) of sEPSCs recorded from ONα-RGCs in wild-type (n = 10) and *B6-DTA* (n = 5) retinas. (C and D) Representative traces (C) and summary data (D) of currents elicited by glutamate puffs in ONα-RGCs in wild-type (1.9 ± 0.07 pS / μm^2) and *B6-DTA* (1.3 ± 0.05 pS / μm^2, p = 2 *10^{-13}) retinas. The area of each application was estimated by 2-photon imaging of a fluorescent dye (Alexa 488) included in the puff solution. Extrasynaptic glutamate receptors may contribute to the currents observed in puff experiments.